12-1-2021

Investigation of human adipose-derived stem-cell behavior using a cell-instructive polydopamine-coated gelatin-alginate hydrogel.

Settimio Pacelli

Aparna R Chakravarti

Saman Modaresi

Siddharth Subham

Kyley Burkey

See next page for additional authors

Investigation of human adipose-derived stem-cell behavior using a cell-instructive polydopamine-coated gelatin-alginate hydrogel

Settimio Pacelli[a] , Aparna R. Chakravarti[b] , Saman Modaresi[b], Siddharth Subham[b], Kyley Burkey[b], Cecilia Kurlbaum[b], Madeline Fang[b], Christopher A Neal[c], Adam J Mellott[c], Aishik Chakraborty[d], Arghya Paul[d]*

Hydrogels can be fabricated and designed to exert direct control over stem cells' adhesion and differentiation. In this study, we have investigated the use of polydopamine (pDA)-treatment as a binding platform for bioactive compounds to create a versatile gelatin-alginate (Gel-Alg) hydrogel for tissue engineering applications. Precisely, pDA was used to modify the surface properties of the hydrogel and better control the adhesion and osteogenic differentiation of human adipose-derived stem cells (hASCs). pDA enabled the adsorption of different types of bioactive molecules, including the model osteoinductive drug (dexamethasone) as well as a model pro-angiogenic peptide (QK). The pDA treatment efficiently retained the drug and the peptide compared to the untreated hydrogel and proved to be effective in controlling the morphology, cell area, and osteogenic differentiation of hASCs. Overall, the findings of this study confirm the efficacy of pDA treatment as a valuable strategy to modulate the biological properties of biocompatible Gel-Alg hydrogels and further extend their value in regenerative medicine.

Introduction

Hydrogels made of natural polymers represent suitable platforms that can be designed to mimic the extracellular matrix microenvironment and control the biological response of stem cells[1]. Precisely, physical, mechanical, and superficial properties of hydrogels dictate the ability of stem cells to adhere, proliferate, and differentiate[2,3]. Understanding the role of each parameter can be useful to fabricate hydrogels with a set of well-defined properties to exert direct control over stem cell morphology, secretion of therapeutic factors, as well as gene expression[4].

An exciting and well-investigated approach to modulate hydrogels' physical and superficial properties is the binding of polydopamine (pDA) on the surface of hydrogels[5]. pDA can be formed easily in alkaline conditions without the need for expensive reagents and can be potentially deposited onto any material such as synthetic and natural polymers[6]. pDA has been used to treat nanomaterials[7] and scaffolds with different designs, shapes, and patterned structure[8,9]. The treatment time, concentration of dopamine, and the method used to bind pDA are all contributing factors that can impact the thickness, hydrophilicity, and roughness of the reactive polymeric film. All these parameters have been widely explored to modulate stem cell adhesion on different types of scaffolds[10,11]. For instance, by varying the roughness of the surface, it is possible to enhance the adsorption of extracellular proteins, thus varying the focal adhesion points of stem cells on the material, which are essential for cell-matrix interactions[12].

Additionally, several research groups have demonstrated how the inclusion of polydopamine enhances the differentiation of stem cells[13–15]. Specifically, this approach has been studied mainly in orthopedic applications involving the use of polymeric scaffolds and titanium-based implants to promote osseointegration and facilitate stem cell osteogenic differentiation[16,17]. For instance, it has been demonstrated that pDA can activate the PI3K transduction signaling pathway involved in the regulation of osteogenic differentiation in periodontal ligament stem cells[18].

One of the advantages of using pDA is also its high chemical reactivity due to the presence of catechol units[19]. Michael additions reactions, as well as Schiff base reactions, can take place in the presence of amine, thiol, hydroxyl, and other nucleophilic functional groups that are present in many proteins and biological molecules[20]. Similarly, the

possibility to control its degree of oxidation[21] and the presence of indole units enables the possibility to establish other non-covalent interactions with biomolecules, including hydrogen bonds, dipole-ion interactions and π-π interaction with aromatic molecules as demonstrated in our previous study[22]. This chemical reactivity enables the possibility to functionalize the surface of hydrogels with a variety of biomolecules ranging from small drugs[23,24], biomimetic peptides[25] to large macromolecules[26]. Needless to say, this strategy can enable the realization of a more bioactive hydrogel platform that can better mimic the extracellular environment and elicit a higher level of control on stem cells' regenerative potential[27].

Based on this premise, we aimed to control the physical and biological properties of a well-known interpenetrating polymeric network based on gelatin and alginate (Gel-Alg) using pDA. Specifically, we have investigated the influence of substrate stiffness and pDA deposition on the cellular response of human adipose-derive stem cells (hASCs). This cell line was selected because of its high proliferative capacity and ease of differentiation into other lineages. The goal was to identify and evaluate the optimal combination of hydrogels' parameters that had a significant impact on hASCs' morphology, cytoskeletal rearrangement, and osteogenic differentiation. Once identified, this set of properties can be selected appropriately to fabricate Gel-Alg scaffolds or polymeric treatment with improved bioactivity that will elicit a direct control on hASCs' response in terms of adhesion, proliferation, and differentiation.

Materials and Methods

Hydrogel synthesis

Hydrogels were fabricated by mixing gelatin type A (Bloom grade 300) and alginate (Mw 1×10^6) in a ratio 10:1 w/w. Briefly, an equal volume of gelatin (11.1% w/v) and alginate (1.1% w/v) solutions in distilled water were mixed at 37 °C prior to the addition of the chemical crosslinkers. N-hydroxysuccinimide (NHS) and 1-Ethyl-3-(3-dimethyl aminopropyl) carbodiimide (EDC) were used to activate the carboxylic groups of alginate and gelatin to enable the formation of amide bonds between the two polymers. Specifically, two degrees of crosslinking were achieved by varying the amount of NHS and EDC. The two reagents were added separately to the polymeric mixture in a 1:1 molar ratio. Low and high crosslinked networks were obtained by introducing EDC and NHS corresponding to the 40% (1.12×10^{-5} moles) and 80% (2.25×10^{-5} moles) of the total moles of carboxylic groups in alginate, respectively. The crosslinkers were mixed for 30 seconds, and then the gels were allowed to fully crosslink for 24 hours. The final concentrations of gelatin (5% w/v) and alginate (0.5% w/v) were kept as constant parameters in each gel formulation.

Rheological, mechanical and physical characterization of the hydrogel

The Gel-Alg networks were characterized by rheological studies. Frequency sweep tests were carried out at 37 °C to test the different degrees of crosslinking. Hydrogels of 3 mm thickness were placed on a serrated plate-plate geometry, and samples were analyzed in the range of frequencies from 0.01 to 10 Hz. Preliminary strain sweep tests were carried out to evaluate the linear viscoelastic region for each sample and identify the optimal strain (1%) to run the frequency sweep analysis. A water trap was placed on top of the hydrogels to avoid excessive evaporation during the test, and three different hydrogels were measured for each group.

Strain sweep tests were performed in the range of strain varying from 0.01% to 200% at 37 °C using a serrated plate-plate geometry. The results were obtained by applying a constant oscillation frequency of 1 Hz. The yield of strain was determined by monitoring the crossover between the storage modulus, G', and the viscous modulus, G". Three different samples were tested for each group. Similarly, following the same experimental conditions, cyclic strain experiments were carried out to evaluate the ability of the hydrogels to recover their initial storage modulus, G'. Specifically, hydrogels were subjected to 1% of strain for 30 seconds, followed by a cycle at 100% of strain for

an additional 30 seconds. These two steps were repeated three times, and the variation of G' values was recorded throughout the analysis.

The compressive modulus of the hydrogels was measured using an RSA-III dynamic mechanical analyzer (TA Instruments, New Castle, DE) and tested under unconfined uniaxial compression with a 35 N load cell (n = 8). The sample diameter was measured using a caliper, and the thickness was calculated directly using the RSA-III. All mechanical analyses were carried out on the swollen Gel-Alg hydrogels, and compression plates were treated with mineral oil to minimize gel drying during the test. Samples were compressed unconstrained to 95% of their original height. A compression rate of 0.0075 mm/sec was used. The compressive modulus, E, for the different groups was measured using the slope of the stress-strain curve in the range of strain varying from 5 to 15 % of strain.

Hydrogel treatment with polydopamine

Gel-Alg hydrogels were treated with a pDA to modulate the surface properties of the different polymeric networks. Briefly, the hydrogels were pre-formed in a 24 well plate following the protocol reported in section 2.1. Several concentrations of dopamine were tested, varying from 1 to 4 mg/mL. Dopamine was solubilized in 10 mM tris buffer (pH=8.5) to allow the polymerization of pDA on the surface of the hydrogels. Specifically, the dopamine solutions (1 mL) were placed in each well containing the hydrogel, and the well plate was shaken at 60 rpm for 1 hour. Then, each dopamine solution was removed and replaced with a fresh tris buffer solution. The gels were washed for 24 hours to remove any unbound dopamine. The hydrogels were either washed with phosphate buffer containing 1% penicillin/streptomycin for cell culture studies or freeze-dried for further surface analysis.

The swelling property of the freeze-dried hydrogels was also tested. Hydrogels were weighed and soaked in phosphate-buffered saline (PBS) (Sigma-Aldrich, St. Louis, MO) at 37°C. The weight of the swollen hydrogels was monitored at different time points, and the study was stopped when an equilibrium of swelling was reached. Specifically, the swelling ratio (%) was calculated using the following equation:

$$\boldsymbol{Swelling\ ratio}\ (\%) = \frac{\boldsymbol{Ws - W_d}}{\boldsymbol{Wd}} \times \mathbf{100}$$

where W_s is the weight of the swollen hydrogel, and W_d indicates the weight of the freeze-dried hydrogel.

Testing pDA binding efficiency to the hydrogel polymeric network: SEM and XPS analysis

Hydrogels with and without a pDA treatment were characterized by scanning electron microscopy (SEM) analysis to visualize the surface and the internal porosity. Freeze-dried samples were mounted on a holder with carbon tape and sputter-coated with gold. A 35 µm thick layer of gold was deposited on each sample. SEM images were taken with a FEI Versa 3D Dual Beam microscope using an acceleration voltage ranging from 1 to 10 kV with an in-lens detector.

Freeze-dried samples with and without a pDA treatment were also characterized by X-ray photoelectron spectroscopy (XPS) analysis using a PHI 5000 VersaProbe II ultrahigh vacuum (1×10^{-9} bar) apparatus equipped with an AlKα X-ray source and a monochromator. Tests were performed with an X-ray beam size of 100 µm. The survey spectra were recorded with pass energy (PE) of 117 eV, a step size of 1 eV, and a dwell time of 20 ms. In contrast, a PE of 23.5 eV, step size of 0.05 eV, and a dwell time of 20 ms were selected as key parameters while recording the high-energy resolution spectra of O 1s and N 1s. Prior to each measurement, an optimal focal point was selected by performing an automated height adjustment to the highest intensity. The optimal signal to noise ratio was obtained by adjusting the number of average sweeps for each element. All the data were processed by a Multipak peak fitting software version 2.3.15.

Biocompatibility studies of formulated pDA-treated hydrogels

Human adipose-derived stem cells (hASCs) (RoosterBio, USA) were cultured in alpha-Minimum Essential Medium (α-MEM) with 15% fetal bovine serum (FBS) (Thermo-Fischer Scientific, USA) and 1% penicillin/streptomycin (Thermo-Fischer Scientific, USA) at 37°C and 5% CO_2. Passages 3–5 were used for all the studies.

Hydrogels were prepared in a 24 well plate following the previous protocol described and washed with PBS supplemented with 1% penicillin/streptomycin. Hydrogels were also soaked in α-MEM, with 15% of FBS prior to seeding with hASCs. Cells were seeded at a density of 2.5 x 10^3 on each gel. hASC were let to proliferate, and an MTS assay was carried out at 24 and 48 hours to evaluate cell proliferation in the different groups. The absorbance of the samples was measured at 490 nm, as for the manufacturer's protocol. The number of hASCs was determined using a standard curve in the range from 2.5 10^3 to 2 x10^4 cells, and the results were expressed as a mean ± standard deviation (n = 5).

Cell morphology was assessed by staining the actin of hASC with Alexa Fluor Phalloidin 488 and the nuclei with 4',6 diamidino-2-phenylindole, dihydrochloride (DAPI). For this specific study, cells were seeded at a density of 1 x 10^3 on each hydrogel. Cells were fixed using 4% paraformaldehyde solution for 5 minutes and washed with PBS (pH 7.4). Then, hASCs were treated with a solution of Triton X-0.1 for 30 minutes, followed by washing with PBS and staining with Alexa Fluor Phalloidin 488 (dilution 1:40 in PBS) and DAPI (1µl/mL in PBS). Images were taken using a fluorescent microscope Zeiss **(Oberkochen, Germany)** at the magnification of 20 and 40X. Quantification of hASCs' cell area was carried out using ImageJ (NIH, USA) by drawing the cell boundaries. The number of actin stress fibers were counted manually for each cell. At least five different cells from 10 different images were used to quantify both parameters. Results were expressed as a mean ± standard deviation.

Determining the stem cell traction forces on the pDA-treated hydrogel surfaces

The hydrogels were prepared by introducing a suspension of microbeads (0.2 µm) in the polymeric mixture to study the hASCs traction forces on Gel-Alg with different stiffness. The beads were diluted 1:10000 to ensure a homogeneous distribution within the polymeric network. 10 µL of the viscous polymeric mixture containing the beads and NHS/EDC in the ratio described previously was placed in the center of a well of a 96 well plate. The well plate was centrifuged at 2,000 rpm for 10 minutes to flatten the drop and cover the surface of each well. The hydrogels were allowed to crosslink for 24 hours. The thickness of the gel was calculated based on the volume of the gel and the area of the 96 well plates. Subsequently, 5 x 10^3 hASCs were seeded on each gel and allowed to grow for 24 hours. Cells were detached from the hydrogel surface using trypsin 0.1%, and fluorescent images of the beads embedded in the polymer network were taken before and after the step of cell removal. Images in the same field of view were taken using an EVOS cell imaging microscope. The displacement induced by the cell traction forces was determined by monitoring the fluorescent positions of the beads in the two sets of images before and after cell removal. The two sets of images correspond to the gel in a stressed and relaxed state. The root means square (RMS) traction was quantified using Matlab (Mathwork Inc.), taking into account the displacement field and the values of compressive modulus for each hydrogel substrate obtained by DMA analysis[28].

Determining the adsorption and release properties of pDA-treated hydrogels for model drugs and peptides

Gel-Alg hydrogels were fabricated in a 24 well plate and treated with a dopamine solution in Tris-HCl buffer 10 mM (pH = 8.5) for 1 hour at 37 °C. Different dopamine concentrations were tested in the range of 1 mg/mL to 4.0 mg/mL. Then, the hydrogels were washed with tris buffer to remove the excess of dopamine from the surface for 24 hours. Hydrogels without any pDA treatment were used as a control group.

A dexamethasone fluorescein isothiocyanate (Dex-FITC) solution (0.3 mL) in PBS (10 µg/mL) was placed on top of each gel for 24 hours in the dark at 37°C. The fluorescence intensity of Dex-FITC was measured before and after the process of physical adsorption to determine the amount of Dex linked on the surface of each hydrogel group.

Five different gels for each group were tested to monitor the adsorption. The amount of unbound Dex-FITC was determined by measuring the fluorescence of the solution at an excitation wavelength of 485 nm and using an emission wavelength of 530 nm. Dex-FITC was selected instead of Dex to avoid the interference caused by the light absorbance of EDC in the same UV of Dex. The hydrogels were washed every 24 hours, with 300 µL of fresh PBS, and the fluorescence of the solution was evaluated over a period of 144 hours. The quantity of Dex-FITC remaining adsorbed to the pDA on the hydrogels was indirectly calculated based on the fluorescence intensity measured from the different washes. A calibration plot of Dex-FITC in PBS ranging from 0.4 µg/mL up to 17.5 µg/mL was used to quantify the percentage of Dex-FITC linked to the surface.

Following a similar procedure, the pro-angiogenic QK derivatized with fluorescein (FITC)-KLTWQELYQLKYKGI-(Amide) or (QK-FITC), was used as a model therapeutic peptide[29–31] and bound to the surface of the hydrogels. Briefly, the hydrogels were soaked for 24 hours under agitation at 60 rpm with a QK-FITC solution in TRIS buffer (pH 8.5) at the concentration of 10 µg/mL. The solution was removed after 24 hours, and the fluorescence intensity was measured using an excitation wavelength of 485 nm and an emission of 530 nm. The quantity of QK-FITC was determined indirectly by comparing the initial fluorescence intensity before and after the process of adsorption to the hydrogels. Hydrogels without any pDA treatment were used as controls. A calibration plot of QK-FITC in PBS ranging from 6.25 µg/mL to 25 µg/mL was used to quantify the unbound QK-FITC and determine the percentage of binding to the hydrogels. The stock solution of QK-FITC (2.5 mg/mL) was solubilized in EtOH and further diluted in PBS, due to the limited solubility of the peptide in PBS at high concentrations. Finally, FBS was also adsorbed on the surface of the different hydrogels following the same procedure. However, the amount of unbound FBS after 24 hours was detected using the Bradford reagent and reading the absorbance at 595 nm. The protein quantification was carried out according to the manufacturer's protocol, and the percentage of protein retained in the hydrogel was determined indirectly by subtracting the amount of protein found in solution in comparison to the original amount before the absorption. Five different samples were tested for each group, and the hydrogels without any pDA were used as controls (n=5). Results have been reported as mean ± standard deviation.

Effect of drug-loaded pDA-treated hydrogels on stem cell differentiation

Three different groups were tested in this study, including a test group, a positive and negative control. The test group (pDA-Dex) consisted of hASCs seeded on Gel-Alg hydrogels treated with pDA followed by Dex adsorption. Briefly, gels were prepared in a 24 well plate, washed with Tris buffer, and treated with dopamine for 1 hour following the condition reported in section 2.3. Hydrogels were washed with PBS for 24 hours to remove the unbound dopamine. Then, a Dex solution (0.1 mM) in water/ethanol (9:1) was added to the gels, and the Dex was allowed to adsorb on pDA for 24 hours at 37°C. The positive and the negative control groups consisted of hASCs seeded on Gel-Alg hydrogels that did not receive any treatment.

Prior to cell seeding, the treated hydrogels of each group were washed with PBS containing 1% of penicillin/streptomycin followed by an incubation step in α-MEM containing 15% fetal bovine serum (FBS) and 1% penicillin/streptomycin at 37°C.

Briefly, 5 x 10^4 hASCs were seeded on the surface of the gels and allowed to grow in α-MEM with 15% FBS for 48 hours up to confluency. Then, the culture conditions were changed according to the respective groups. Specifically, the pDA-Dex and negative control group were cultured in media, which consisted of α-MEM supplemented with 50 µM 2-phosphate ascorbic acid and 10 mM β-glycerophosphate and 10% FBS. On the contrary, the positive group was treated with osteogenic media (50 µM 2-phosphate ascorbic acid, 10 mM β-glycerophosphate, 10% FBS, and 10 nM Dex). The media was changed every other day for the whole duration of the study. At 7 and 14 days, gels were stained to investigate the presence of alkaline phosphatase (ALP) using the protocol provided by the manufacturer (Alkaline Phosphatase kit, Sigma Aldrich, USA). ALP enzymatic activity was measured at days 7 and 14 following a fluorometric assay (Abcam, catalog number: ab83371). hASCs were detached

from the surface of the hydrogels using 250 U/mL collagenase type IV at day 7 and 14 of cell culture. Cells were centrifuged at 1,500 rpm for 5 minutes, and the supernatant was removed. Cells were homogenized in ALP buffer following the steps described in the protocol provided by the kit. Fluorescence was measured using a microplate reader at the excitation of 360 nm and an emission wavelength of 440 nm. Five different samples for each group were tested to quantify the amount of ALP.

Alizarin Red staining was evaluated at 14 and 21 days. The cells were fixed with 4% paraformaldehyde and washed three times with water, followed by incubation with a solution of Alizarin Red at the concentration of 2% w/v for 20 minutes. The cells were washed three times with water to remove the excess of staining. Bright-field images were taken to visualize the intracellular calcium deposition. Moreover, calcium quantification was determined using a colorimetric calcium quantification kit (Cayman, catalog number: 701220) at days 14 and 21. Cells were detached from the hydrogel using a collagenase solution 250 U/mL in PBS and centrifuged at 1,000 g for 10 minutes. Cell lysates were obtained using the buffer provided by the kit, and five different samples for each group were analyzed using the colorimetric kit.

Finally, qPCR studies were carried to evaluate the expression of several osteogenic genes, including *ALP*, and *RUNX2*, using GAPDH as the control gene. mRNA from the different samples were extracted using a RNeasy Mini Kit (Qiagen) on day 7, day 14, and day 21, according to the manufacturer protocols. mRNA concentration was quantified using a NanoDrop (Thermo Scientific), and 100 ng of mRNA was used for each sample for its conversion to cDNA. This step was obtained using the High-Capacity cDNA conversion Kit (Applied Biosystems, USA). All primers used were pre-designed KiCqStart SYBR Green primers (Sigma-Aldrich, USA). KiCqStart SYBR Green Master Mix (Sigma-Aldrich, USA) was utilized in each reaction. Specifically, 10 µL of Master Mix was mixed with 2 µL of reversed and forward primers, and 1µL of cDNA obtained from the previous step. Water was added to reach a final volume of 20 µL. All qPCR reactions were performed using a Mastercycler Realplex4 (Eppendorf, Germany). The fold increase expression was calculated using the ΔΔCt relative method, and data were normalized based on the level expression of genes found in the group of hASCs cultured on the gel in basal media at day 7. Three samples for each group were analyzed, and the results were reported as mean ± standard deviation (n=3).

***In vivo* biocompatibility testing of pDA-treated hydrogels**

All procedures were conducted according to the approved Institutional Animal Care and Use Committee (IACUC) protocol (ACUP #2017-2394). A total of eight Sprague Dawley female rats (n = 8) were obtained from Charles River.

The rats were placed under a general anesthetic using Isoflurane. Fur was clipped to expose the back and sides of the animal. Animals were weighed and injected subcutaneously with 0.002 mL of 1 mg/mL Ketofen per gram of body weight. Three alternating scrubs of betadine and alcohol were applied to the surgical sites of each animal. Animals were secured to a nose cone emitting Isoflurane and placed on a surgical pad. A total of four full-thickness 1 cm x 1 cm x 0.5 cm wound defects were made on the back of each animal. Hydrogel scaffolds (1 cm x 1 cm x 0.5 cm) composed of Gelatin Type A, Alginate, NHS [N-hydroxysuccinimide], and EDC [1-ethyl-3-(3-dimethylaminoprpyl] were implanted in the two left wounds of the animals. Similarly, the same hydrogel scaffolds, treated with polydopamine and QK peptide, were implanted in the two left wounds of the animals. Each animal did not receive any hydrogel in the right two wounds. All wounds were closed using 4-0 Vicryl sutures (Ethicon, Sommerville, NJ) using a simple continuous technique. Each wound site was closed with 3-4 bites. Elizabethan-collars (Braintree Scientific, Inc., Braintree, MA) were installed securely on each animal to prevent access to surgical sites for 24 hours. All animals were monitored after surgeries until fully recovered with ambulatory function. After 15 days, animals were placed under a general anesthetic using Isoflurane. Animals were euthanized via injection with Beuthanasia®-D CIIIN (MERK, Kenilworth, NJ) at a dose of 270 mg/kg body weight, followed by decapitation. All wound sites were excised and placed in RNALater (Qiagen) followed by cryo-preservation at -80°C for

downstream applications. Samples cryo-preserved in RNALater (Qiagen) were thawed overnight at 4°C. Samples were washed in PBS three times, and fixed in 4% paraformaldehyde in PBS for 1 hour. Samples were washed in PBS twice, followed by gradient dehydration. Samples were cleared in Histo-Clear (National Diagnostics, Atlanta, GA), and embedded in paraffin and serial-sectioned at a thickness of 10 μm and mounted on SuperFrost glass slides (Thermo Fisher Scientific, Waltham, MA). Sections were stained with H&E to observe the cellular and tissue response to various treatments in the wound defects. Four different animals per group were examined (n=4).

Statistical analysis

Statistical analysis was performed using one-way analysis of variance (ANOVA) followed by Tukey's multiple comparison test used to determine whether a significant difference existed between specific groups. A T-test was carried out when comparing the mean of sets of data. All statistical analyses were carried out with GraphPad Prism Software 6. A *p*-value less than 0.05 indicates statistical significance, which was displayed as * = $p < 0.05$, ** = $p < 0.01$, *** = $p < 0.001$.

Results and discussion

Hydrogel design and effect of substrate stiffness on hASCs

Gelatin type A and alginate were selected as natural biocompatible polymers to fabricate a model hydrogel already investigated by our research group to treat ceramic-based scaffolds[32]. In our previous study, we have proved that the hydrogel treatment could withstand cyclic compression and prevent the brittle ceramic scaffold from being structurally damaged. Additionally, the hydrogel treatment could be used as a carrier for the delivery of model proteins and enabled hASCs adhesion and proliferation. However, the hydrogel itself did not seem to exert any control over hASCs osteogenic differentiation, which was enhanced only in the presence of the osteoconductive β-TCP scaffold.

To further expand on the potential of this hydrogel platform as a modulator of hASCs' behavior, the stiffness of the hydrogels was varied by modifying the degree of crosslinking. Alginate can establish electrostatic interactions with the positively charged Gelatin type A at physiological pH. Aside from physical interactions, gelatin and alginate can also be crosslinked using NHS/EDC chemistry (Fig. 1A). The degree of crosslinking can be modulated by varying the concentration of NHS/EDC to obtain hydrogels with different stiffness, as previously demonstrated[32]. To evaluate this parameter, physical and mechanical properties were tested by monitoring changes in swelling, porosity, and mechanical properties. The increase in the degree of crosslinking had a profound effect on the physical and mechanical features of the scaffold. The presence of a high degree of crosslinking significantly reduced the degree of swelling, probably due to the limited extensibility of the polymeric chains. Interestingly, the swelling profiles were similar for the first two hours, although the samples containing a low degree of interconnectivity displayed higher values and reached a plateau after 4 hours (Fig. 1B). The variation in the extent of crosslinking was also demonstrated by SEM analysis, which revealed the presence of smaller and more homogeneous pores in the high degree samples compared to low hydrogels (Fig. 1C). These differences were confirmed by rheological analysis, which is a useful investigation strategy to indirectly determine the different degrees of interconnectivity within a polymeric network. Frequency and strain sweep tests showed how the increased degree of crosslinking had a direct impact on the hydrogels' stiffness and mechanical performance. The high samples displayed increased values of storage modulus, G', which is indicative of a stiffer material (Fig. 1D). Similarly, the same hydrogels (high) were more mechanically resistant and displayed failure for the higher value of strain. Specifically, the crossover between the storage modulus, G', and the viscous modulus, G", occurred at around 50% of strain for the low hydrogels while the high system could withstand a strain close to 100% of strain (Fig. 1E). Both formulations could recover their original storage modulus after being subjected to cyclic strains. However, at 100% of the strain, it was possible to observe how the high samples were able to recover faster after the initial drop in the value of G', especially in the

first two cycles. Finally, compressive tests were carried out to calculate the compressive moduli of the scaffolds. Fig. 2A shows the behavior of the scaffold under compressive stress. In accordance with the rheological results, a significant increase in the Young's Modulus from 11.3 ± 1.3 kPa to 15.4 ± 1.7 kPa was observed when comparing the low and high samples, respectively (Fig. 2A). Overall, these findings suggest that the amount of EDC and NHS affected the physical and mechanical properties of the scaffolds, generating two sets of hydrogels with a distinct level of stiffness.

However, it was essential to define whether this change was enough to affect hASCs proliferation and morphology. hASCs have been selected as a model stem cell line due to their high proliferation capacity and osteogenic-differentiation potential, as demonstrated in other hydrogel scaffolds[33].

The selected hydrogel enabled stem cell adhesion and proliferation due to the presence of gelatin, which contains the cell binding sequence RGD found in many extracellular matrix proteins, including fibronectin, laminin, and vitronectin. Additionally, the selected hydrogel model has already been proved to be biocompatible *in vivo*[34]. hASCs were able to spread and proliferate easily within 48 hours, although stiffness did not affect either their morphology or their proliferation capacity (Fig. 2B and 2C). Similarly, cell area analysis showed that varying the degree of crosslinking did not influence cell area significantly with similar values between the two groups (Fig. 2D).

These results suggest that the degree of interconnectivity between the gelatin polypeptide chains as well as among the two polymers did not play a significant role in modifying the initial cell-matrix adhesion and proliferation process, probably because cells were seeded on the surface of the hydrogel. However, it is worth noticing that hASCs were able to exert higher tractional forces on the surface of the stiffer gels because of the different degrees of elasticity (Fig. 2E and 2F). Such an increase in tractional forces has been proven for other types of other natural and synthetic polymeric hydrogels with different degrees of crosslinking[35]. Moreover, it is well established that hydrogels' stiffness can modulate cellular differentiation potential, and specifically stiffer matrices can indirectly guide stem cells towards osteogenic differentiation[36,37]. Since the goal of this research was to identify the optimal conditions to create an osteogenic hydrogel treatment, the hydrogel with the higher stiffness was selected moving forward in the rest of the study.

Influence of pDA-treated hydrogels on hASC morphology

Aside from modifying the stiffness of the scaffold, it was essential to vary the superficial properties of the hydrogels. Samples with the highest stiffness were subjected to pDA treatment using different concentrations of dopamine. After the treatment, pDA looked evenly distributed on the hydrogel's surface with an increasing dark brown color based on the initial concentration of dopamine used before the polymerization (Fig. 3A). Fig. 3B demonstrates the adhesivity of the pDA treated hydrogel. The schematic shows the applicability of such material. This adhesive formulation can be used as a scaffold for wound healing. Additionally, the photographs display the mechanical resilience of the material.

XPS analysis was carried out to confirm the presence of a pDA on the surface. Precisely, the N s1 spectrum showed the presence of a peak at 399.8 eV, which could not be found in the hydrogel without any pDA (Fig. 3C). The same signal, which is characteristic of amine (-NH) bond present in pDA, has also been detected in other reports investigating polymeric system treated with pDA[39]. Finally, SEM analysis of the hydrogels' surface did not show any visible changes in the surface after the pDA treatment, probably because the overall process was performed only for one hour (Fig. S1A-D). This result is consistent with other research that reported a change in the surface morphology only when the treatment procedure was prolonged for longer than one hour[38,39].

We also investigated the effect of the polydopamine treatment on hASCs' morphology, and we observed a substantial increase in the cell area as the concentration of dopamine was increased (Fig. 3D and 3E). Similar outcomes were found in our previous report using hASCs on gellan gum-based hydrogels[40], as well as in other research investigating endothelial cells area on synthetic polymeric scaffolds treated with pDA at different times[41].

Additionally, we observed an increase in the number of actin filaments in hASCs seeded on the hydrogels treated with pDA formed with the highest amount of dopamine (4 mg/mL) (Fig. 3F). Generally, this increase in the number and length of actin filaments is associated with a large number of focal adhesion points, as reported in another study using hASCs on electrospun polylactic fibers[42]. The increase in cell area and length of cytoskeletal filaments suggests an enhancement in the cell adhesion properties to the substrate, which could be attributed to the increased absorption on the hydrogel surface of serum proteins present in the media promoted by pDA. For instance, in another report, pDA was able to augment the adsorption of bovine serum albumin (BSA) on polyvinyl alcohol and polyacrylamide hydrogels, significantly[43]. Therefore, we investigated whether the amount of protein adsorbed on the surface of the hydrogels was different based on the pDA treatment. Interestingly, we found an increase of FBS adsorption in the hydrogel treated with pDA (1 mg/mL), although this change was not statistically significant among the test groups (Fig. S2). It should also be noted that changes in cytoskeletal structure, surface area, and focal adhesion can also be responsible for the activation of a focal adhesion signaling pathway that enhances osteogenic differentiation in hASCs and other types of stem cells without the use of any osteoinductive factors[38,42]. Overall, these results indicate that for this hydrogel system, the inclusion of pDA could impact stem cell morphology to a greater extent than substrate stiffness.

Assessment of pDA-treated hydrogels as a versatile platform for sustained delivery of model drugs

Besides the hydrogel's intrinsic ability to modulate cellular morphology as demonstrated above, pDA treatment can also be used to affect the biological properties of scaffolds. For instance, many studies have explored the use of pDA to covalently link adhesive or osteogenic peptides[43,44] as well as angiogenic growth factors[45]. Due to the presence of catechol units, the pDA treatment can participate in a variety of chemical interactions, including Michael addition and Schiff base reactions with amine and thiol functional groups of proteins. Similarly, the aromatic structure of the quinone in the pDA chain can participate in π-π interactions with aromatic compounds.

For instance, we examined the possibility of binding dexamethasone as a model molecule to promote osteogenic differentiation of hASCs (Fig. 4A). In this case, the drug, which is a corticosteroid molecule, can be adsorbed mostly by π-π interaction with pdA, as reported in our previous study[22]. The pDA treatment enabled the retention of dexamethasone over time with a limited drug loss of approximately 19 ± 1% of the initial adsorbed drug after 6 days.

On the contrary, without the pDA treatment, a significant decrease in dexamethasone of almost 84±2% of the original amount was detected in the same time frame (Fig. 4B). These results indirectly confirm the physical adsorption of the drug on the pDA-treated hydrogel.

The initial amount of dopamine for the pDA treatment also seemed to affect the percentage of drug retained after 6 days. Precisely, 69±1% and 81±2% of the initial drug adsorbed was still retained in the pDA-treated hydrogels made with 1 mg/mL and 2 mg/mL of dopamine after 6 days, respectively (Fig. S3A and S3B). However, further increasing the concentration of dopamine (4 mg/mL) did not significantly impact the amount of drug adsorbed. hASCs were then seeded on the hydrogels, and their osteogenic differentiation was assessed for 21 days. Three different groups were tested to evaluate whether the drug was still active after being adsorbed on the hydrogel. Notably, osteogenic differentiation was confirmed after 14 and 21 days in the test group (pDA-Dex) without the addition of any osteogenic factors. Alkaline phosphatase activity was monitored over the course of two weeks to assess the initial process of osteogenic differentiation, as reported in other studies. (Fig. 4B and C). hASCs in the test group displayed a level of osteogenic differentiation similar to the positive control, indicating that the drug was efficiently retained and was still active. Additionally, intracellular calcium deposits were assessed both qualitatively and quantitatively after 21 days (Fig. 4D and 4E). Similar to ALP results, calcium content was similar to the positive group where hASCs were exposed throughout the experiment to Dex in the media. Finally, the osteogenic differentiation of hASCs was also investigated at the gene level by studying the upregulation of ALP and RUNX2.

Both genes were upregulated in the pDA-Dex system compared to the negative control group at all times tested (Fig. 4G and 4H). This finding confirmed the hASCs commitment towards the osteogenic lineage once cultured on pDA-Dex substrates without the need for the introduction of any osteogenic factor in the media. Another critical aspect to consider when designing a hydrogel treatment for osteogenic applications is the possibility to control its angiogenic properties. Angiogenesis needs to be accurately regulated since it plays a critical role in the process of bone remodeling. Therefore, we took advantage of the chemical reactivity of pDA and explored the possibility of linking a well-known pro-angiogenic peptide, namely QK peptide. This is a short peptide of 2.1 kDa designed based on the active structure of VEGF-A. This short peptide sequence mimics the α-helical receptor-binding region-specific to VEGF[46]. The QK peptide is known to promote the proliferation of endothelial cells in vitro and exhibits competitive binding to VEGF receptors[46–48]. Consequently, for all these reasons, the QK peptide was selected as a promising bioactive molecule that could be bound to pDA to promote endothelial activation and capillary-like formation *in vivo*.

Firstly, we investigated the *in vitro* potential of the peptide to promote human umbilical vein endothelial cells (HUVECs) proliferation at different concentrations to identify the optimal amount of peptide to bind to pDA. The peptide at the concentration of 10 μg/mL was able to promote HUVEC proliferation after 24 hours with comparable results to the positive group where the cells were cultured in media containing both VEGF and bFGF (Fig. S4A). No significant difference was observed when increasing the concentration of the peptide in the media up to 20 μg/mL. Additionally, the increase in cell proliferation was also confirmed by the upregulation of three pro-angiogenic markers such as VEGFR1, VEGFR2, and NP1, which are usually activated by VEGF stimulation (Fig. S4B). Our findings are similar to other studies researching the biological activity of the QK peptide[49]. The QK peptide was adsorbed on the surface of the hydrogel with the help of pDA. Based on other reports investigating the linkage of peptides containing lysine residues at different pH on pDA[50], it is likely that the peptide can establish Schiff base bonds with the quinone structure of pDA. This is particularly true in alkaline environments similar to the one used in this study (TRIS buffer with a pH value of 8.5). However, we cannot exclude the possibility of hydrogen bonds with the catechol structure of pDA as an additional possible mechanism for the process of binding.

The efficiency of peptide binding was quantified indirectly by measuring the fluorescence of the unbound peptide QK-FITC (Fig. S4C). After 24 hours, around 85% of the total amount of peptide was adsorbed on the surface of the hydrogel. The extent of peptide retention on the hydrogel was similar in all the samples tested irrespective of the initial concentration of dopamine used for the pDA treatment (Fig. S4C).

The hydrogels modified with the QK peptide and pDA were tested *in vivo* in a wound healing rat model. The hydrogels were placed subcutaneously in the dorsal side of the rats, and the healing process was compared with sham controls (untreated) and animals receiving the blank hydrogels (Fig. 5A). Fig. 5B displays images showing that all the wounds were able to heal completely after 15 days post-surgery, and no inflammation was visible in the skin of all the group tested except for a minor swelling around their left-wound sites where pDA-QK hydrogels were implanted. Interestingly, H&E staining showed no cell infiltration into the hydrogel structure, which remained intact until 15 days post-surgery. In contrast, a major degree of degradation was observed in the pDA-QK system suggesting a process of remodeling during the wound healing process. However, no capillaries were formed withing the hydrogel structure. Therefore, based on these findings, further investigation needs to be carried out to ascertain the angiogenic potential of the hydrogel and better understand the correlation between the *in vivo* degradation and the hydrogel treated with pDA.

Conclusions

In summary, the findings of this research demonstrate how the physical and biological properties of well-investigated hydrogels can be further enhanced using polydopamine. Specifically, we were able to advance the

regenerative potential of a well-known hydrogel platform previously investigated as a treatment for ceramic-based scaffolds. Firstly, the pDA treatment exerted direct control over the cytoskeletal remodeling of hASCs by promoting an increase in cell area and the number of actin filaments, which were directly influenced by the concentration of dopamine used for the pDA treatment. In contrast, this effect was not evident when varying the stiffness of the scaffold, although the change in elasticity was
responsible for an increase in cellular traction forces. The pDA was also able to promote retention of the osteoinductive drug dexamethasone. The biological activity of the drug was retained after the adsorption, and the Dex-pDA hydrogel enabled the osteogenic differentiation of hASCs without the use of any additional osteogenic factor in the media. Finally, the pDA treatment also allowed the adsorption of the pro-angiogenic peptide QK in the hydrogel. The peptide was efficient in promoting endothelial proliferation and upregulation of several angiogenic markers *in vitro*; however, when tested *in vivo*, no significant increase in angiogenesis was detected compared to the other groups. Further optimization in the porosity and degradability of the scaffold may be necessary to promote cellular infiltration, which was likely the limiting factor for the observed results *in vivo*.

Conflict of interest

The authors declare no conflict of interest.

Acknowledgments

A.P. is grateful to the funding and supports from Canada Research Chairs Program of the Natural Sciences and Engineering Research Council (NSERC) of Canada, NSERC Discovery Grant, NSERC Discovery Accelerator Supplements (DAS), New Frontiers in Research Fund (NFRF) - Exploration Stream, and Wolfe-Western Fellowship At-Large for Outstanding Newly Recruited Research Scholar. The authors would also like to acknowledge Shruthi Polla Ravi for her help with the artwork. The authors also acknowledge the company, BioRender. Illustrations were created with BioRender.com.

References

1 W. L. Murphy, T. C. McDevitt and A. J. Engler, *Nature Materials*, 2014, 13, 547–557.

2 C. Cha, W. B. Liechty, A. Khademhosseini and N. A. Peppas, *ACS Nano*, 2012, 6, 9353–9358.

3 A. M. Schaap-Oziemlak, P. T. Kühn, T. G. van Kooten and P. van Rijn, *RSC Advances*, 2014, 4, 53307–53320.

4 Y. H. Tsou, J. Khoneisser, P. C. Huang and X. Xu, *Bioactive Materials*, 2016, 1, 39–55.

5 L. Han, L. Yan, K. Wang, L. Fang, H. Zhang, Y. Tang, Y. Ding, L. T. Weng, J. Xu, J. Weng, Y. Liu, F. Ren and X. Lu, *NPG Asia Materials*, 2017, 9, 372.

6 Y. H. Ding, M. Floren and W. Tan, *Biosurface and Biotribology*, 2016, 2, 121–136.

7 I. S. Kwon, G. Tang, P. J. Chiang and C. J. Bettinger, *ACS Applied Materials and Interfaces*, 2018, 10, 7681–7687.

8 D. Sharma, W. Jia, F. Long, S. Pati, Q. Chen, Y. Qyang, B. Lee, C. K. Choi and F. Zhao, *Bioactive Materials*, 2019, 4, 142–150.

9 K. M. Beckwith and P. Sikorski, *Biofabrication*, 2013, 5, 045009.

10 S. H. Ku, J. S. Lee and C. B. Park, *Langmuir*, 2010, 26, 15104–15108.

11 Y. J. Chuah, Y. T. Koh, K. Lim, N. v. Menon, Y. Wu and Y. Kang, *Scientific Reports*, 2015, 5, 1–12.

12 Y. L. Cheng, Y. W. Chen, K. Wang and M. Y. Shie, *Journal of Materials Chemistry B*, 2016, 4, 6307–6315.

13 X. Shi, L. Li, S. Ostrovidov, Y. Shu, A. Khademhosseini and H. Wu, *ACS Applied Materials and Interfaces*, 2014, 6, 11915–11923.

14 K. Yang, J. S. Lee, J. Kim, Y. bin Lee, H. Shin, S. H. Um, J. B. Kim, K. I. Park, H. Lee and S. W. Cho, *Biomaterials*, 2012, 33, 6952–6964.

15 L. Ge, Q. Li, Y. Huang, S. Yang, J. Ouyang, S. Bu, W. Zhong, Z. Liu and M. M. Q. Xing, *Journal of Materials Chemistry B*, 2014, 2, 6917–6923.
16 L. Jia, F. Han, H. Wang, C. Zhu, Q. Guo, J. Li, Z. Zhao, Q. Zhang, X. Zhu and B. Li, *Journal of Orthopaedic Translation*, 2019, 17, 82–95.
17 D. J. Lee, Y. T. Lee, R. Zou, R. Daniel and C. C. Ko, *Scientific Reports*, 2017, 7, 1–14.
18 J. S. Lee, J.-K. Yi, S. Y. An and J. S. Heo, *Cellular Physiology and Biochemistry*, 2014, 34, 1824–1834.
19 J. Liebscher, R. Mrówczyński, H. A. Scheidt, C. Filip, N. D. Haìdade, R. Turcu, A. Bende and S. Beck, *Langmuir*, 2013, 29, 10539–10548.
20 J. H. Ryu, P. B. Messersmith and H. Lee, *ACS Applied Materials and Interfaces*, 2018, 10, 7523–7540.
21 S. K. Madhurakkat Perikamana, J. K. Lee, Y. M. Shin, T. Ahmad, S. J. Kim, K. M. Park and H. Shin, *Journal of Materials Chemistry B*, 2017, 5, 8865–8878.
22 S. Pacelli, K. Rampetsreiter, S. Modaresi, S. Subham, A. R. Chakravarti, S. Lohfeld, M. S. Detamore and A. Paul, *ACS Applied Materials and Interfaces*, 2018, 10, 24955–24962.
23 H. Li, B. Luo, W. Wen, C. Zhou, L. Tian and S. Ramakrishna, *Materials Science and Engineering C*, 2017, 70, 701–709.
24 C.-H. Yeh, Y.-W. Chen, M.-Y. Shie and H.-Y. Fang, *Materials*, 2015, 8, 4299–4315.
25 E. Ko, K. Yang, J. Shin and S. W. Cho, *Biomacromolecules*, 2013, 14, 3202–3213.
26 S. M. Kang, N. S. Hwang, J. Yeom, S. Y. Park, P. B. Messersmith, I. S. Choi, R. Langer, D. G. Anderson and H. Lee, *Advanced Functional Materials*, 2012, 22, 2949–2955.
27 E. Ko, J. S. Lee, H. Kim, S. Y. Yang, D. Yang, K. Yang, J. Lee, J. Shin, H. S. Yang, W. Ryu and S. W. Cho, *ACS Applied Materials and Interfaces*, 2018, 10, 7614–7625.
28 J. P. Butler, I. M. Toli-Nørrelykke, B. Fabry and J. J. Fredberg, *American Journal of Physiology - Cell Physiology*, 2002, 282, 595–605.
29 L. de Rosa, R. di Stasi and L. D. D'Andrea, *Archives of Biochemistry and Biophysics*, 2018, 660, 72–86.
30 T. Flora, I. G. de Torre, M. Alonso and J. C. Rodríguez-Cabello, *Journal of Materials Science: Materials in Medicine*, 2019, 30, 1–12.
31 K. Hosoyama, C. Lazurko, M. Muñoz, C. D. McTiernan and E. I. Alarcon, *Frontiers in Bioengineering and Biotechnology*, 2019, 7, 205.
32 S. Pacelli, S. Basu, C. Berkland, J. Wang and A. Paul, *Cellular and Molecular Bioengineering*, 2018, 11, 211–217.
33 S. Pacelli, R. Maloney, A. R. Chakravarti, J. Whitlow, S. Basu, S. Modaresi, S. Gehrke and A. Paul, *Scientific Reports*, 2017, 7, 1–15.
34 C. Yang, H. Frei, F. M. Rossi and H. M. Burt, *Journal of Tissue Engineering and Regenerative Medicine*, 2009, 3, 601–614.
35 M. Guvendiren and J. A. Burdick, *Nature Communications*, 2012, 3, 1–9.
36 S. J. Tan, J. Y. Fang, Z. Yang, M. E. Nimni and B. Han, *Biomaterials*, 2014, 35, 5294–5306.
37 W. Zhao, X. Li, X. Liu, N. Zhang and X. Wen, *Materials Science and Engineering C*, 2014, 40, 316–323.
38 N. G. Rim, S. J. Kim, Y. M. Shin, I. Jun, D. W. Lim, J. H. Park and H. Shin, *Colloids and Surfaces B: Biointerfaces*, 2012, 91, 189–197.
39 S. H. Ku and C. B. Park, *Biomaterials*, 2010, 31, 9431–9437.
40 S. Pacelli, P. Paolicelli, S. Petralito, S. Subham, D. Gilmore, G. Varani, G. Yang, D. Lin, M. A. Casadei and A. Paul, *ACS Applied Bio Materials*, 2020, DOI:10.1021/acsabm.9b00989.
41 J. L. Wang, K. F. Ren, H. Chang, F. Jia, B. C. Li, Y. Ji and J. Ji, *Macromolecular Bioscience*, 2013, 13, 483–493.
42 C. C. Lin and S. J. Fu, *Materials Science and Engineering C*, 2016, 58, 254–263.

43 Y. Wu, C. Yu, M. Xing, L. Wang and G. Guan, *Journal of Biomedical Materials Research Part B: Applied Biomaterials*, 2020, 108, 117–127.
44 W. Li, Y. Zheng, X. Zhao, Y. Ge, T. Chen, Y. Liu and Y. Zhou, *PLOS ONE*, 2016, 11, e0150294.
45 Y. M. Shin, Y. bin Lee, S. J. Kim, J. K. Kang, J. C. Park, W. Jang and H. Shin, *Biomacromolecules*, 2012, 13, 2020–2028.
46 L. D. D'Andrea, G. Iaccarino, R. Fattorusso, D. Sorriento, C. Carannante, D. Capasso, B. Trimarco and C. Pedone, *Proceedings of the National Academy of Sciences of the United States of America*, 2005, 102, 14215–14220.
47 K. Zhang, A. Sugawara and D. A. Tirrell, *ChemBioChem*, 2009, 10, 2617–2619.
48 J. E. Leslie-Barbick, J. E. Saik, D. J. Gould, M. E. Dickinson and J. L. West, *Biomaterials*, 2011, 32, 5782–5789.
49 F. Finetti, A. Basile, D. Capasso, S. di Gaetano, R. di Stasi, M. Pascale, C. M. Turco, M. Ziche, L. Morbidelli and L. D. D'Andrea, *Biochemical Pharmacology*, 2012, 84, 303–311.
50 H. Lee, J. Rho and P. B. Messersmith, *Advanced Materials*, 2009, 21, 431–434.

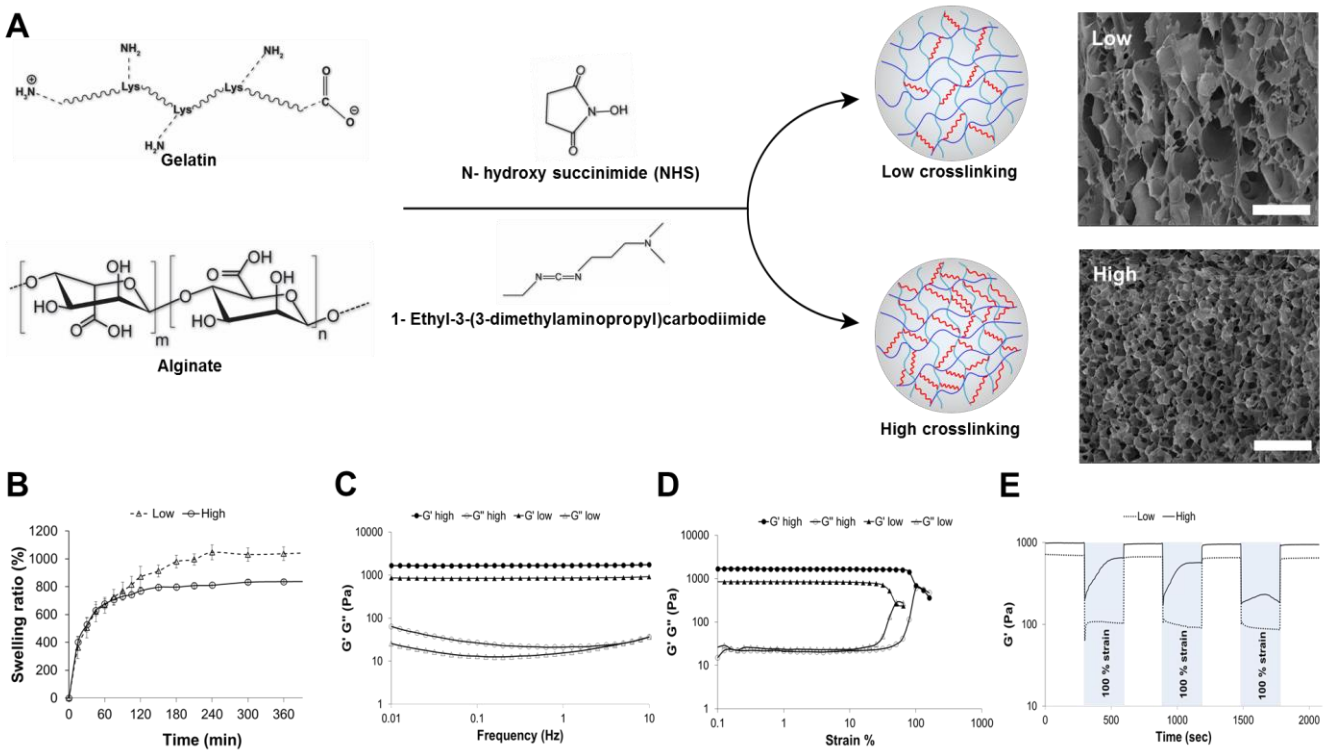

Fig. 1. Gel-Alg hydrogel physical and mechanical characterization. **A)** The schematic is representing the process of chemical crosslinking used to prepare the hydrogels. High and Low crosslinked hydrogels were synthesized by varying the concentration of NHS and EDC. On the bottom corresponding SEM images displaying the internal porosity of the hydrogels. Scale bar = 100 µm. **B)** Swelling profiles of high and low crosslinked hydrogels in PBS (pH 7.4) at 37 ºC (n=3). **C)** Frequency sweep profiles of high and low crosslinked hydrogels in the range of frequencies from 0.01 to 10 Hz. **D)** Representative strain sweep profiles carried out to identify the maximum strain percentage the designed hydrogels can sustain based on their degree of crosslinking. **E)** Representative strain cycle curves displaying the variation in the storage modulus G' as a function of time.

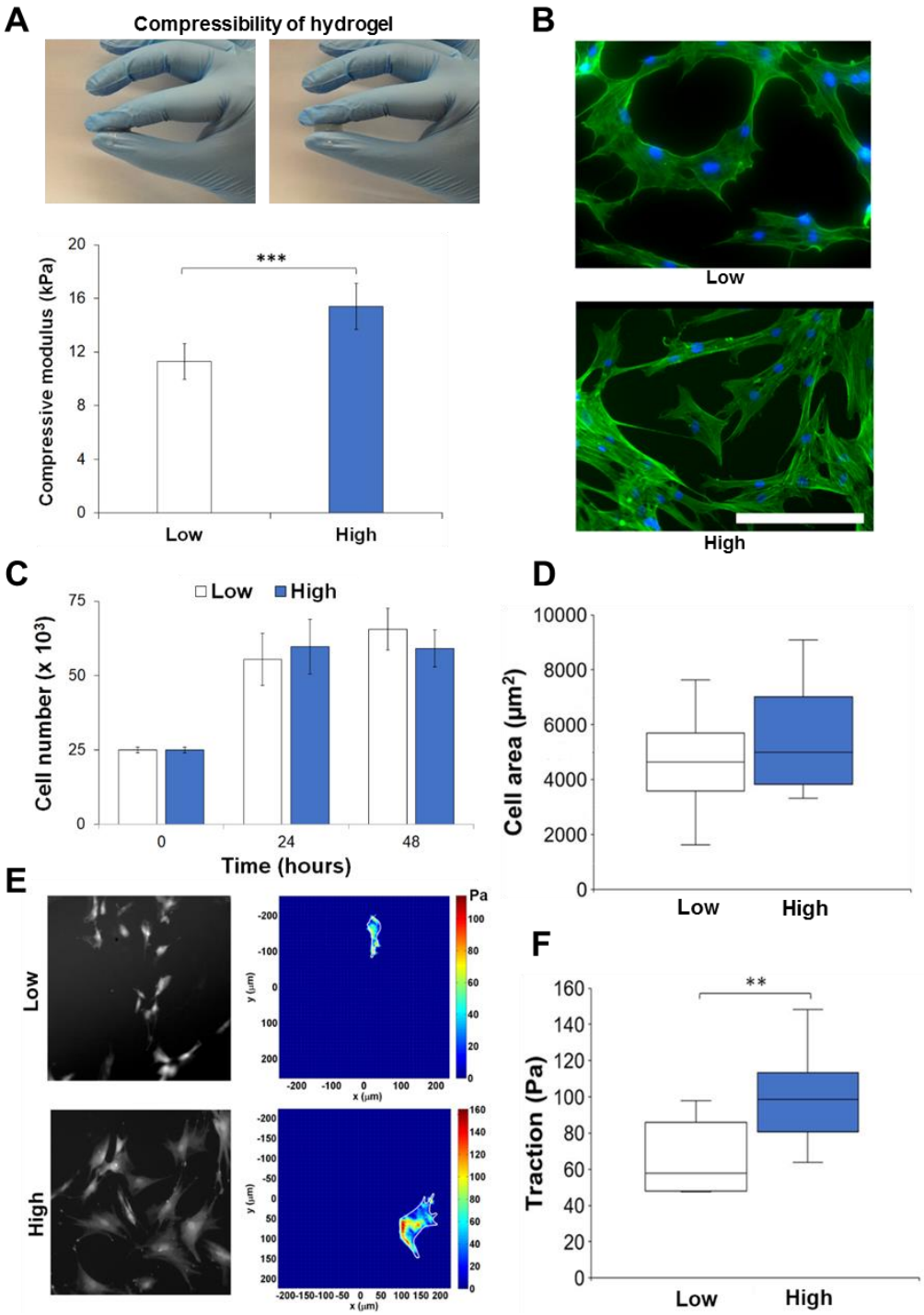

Fig. 2. Assessment of Gel-Alg hydrogel stiffness on hASCs morphology and traction forces. **A)** Image displays the compressibility of the hydrogel. Bottom panel shows the compressive modulus values obtained by compressing the hydrogels with different crosslinked degrees. **B)** Actin-DAPI staining of hASCs seeded on low and high crosslinked Gel-Alg hydrogels after 24 hours of culture. Scale bar = 400 µm. **C)** hASCs proliferation at 24 and 48 hours quantified by MTS analysis. Results are reported as mean ± standard deviation (n=5). **D)** Quantification of cell area by imageJ analysis. 5 separate images at 20X were used to quantify the cell area (n=10). Results are not statistically significant. **E)** Phase contrast pictures and traction map images of hASCs seeded on low and high crosslinked hydrogels. **F)** Rootmean-square (RMS) traction values of hASCs seeded on the two different hydrogel substrates (n=10). ** = $p<0.01$ and *** = $p<0.001$.

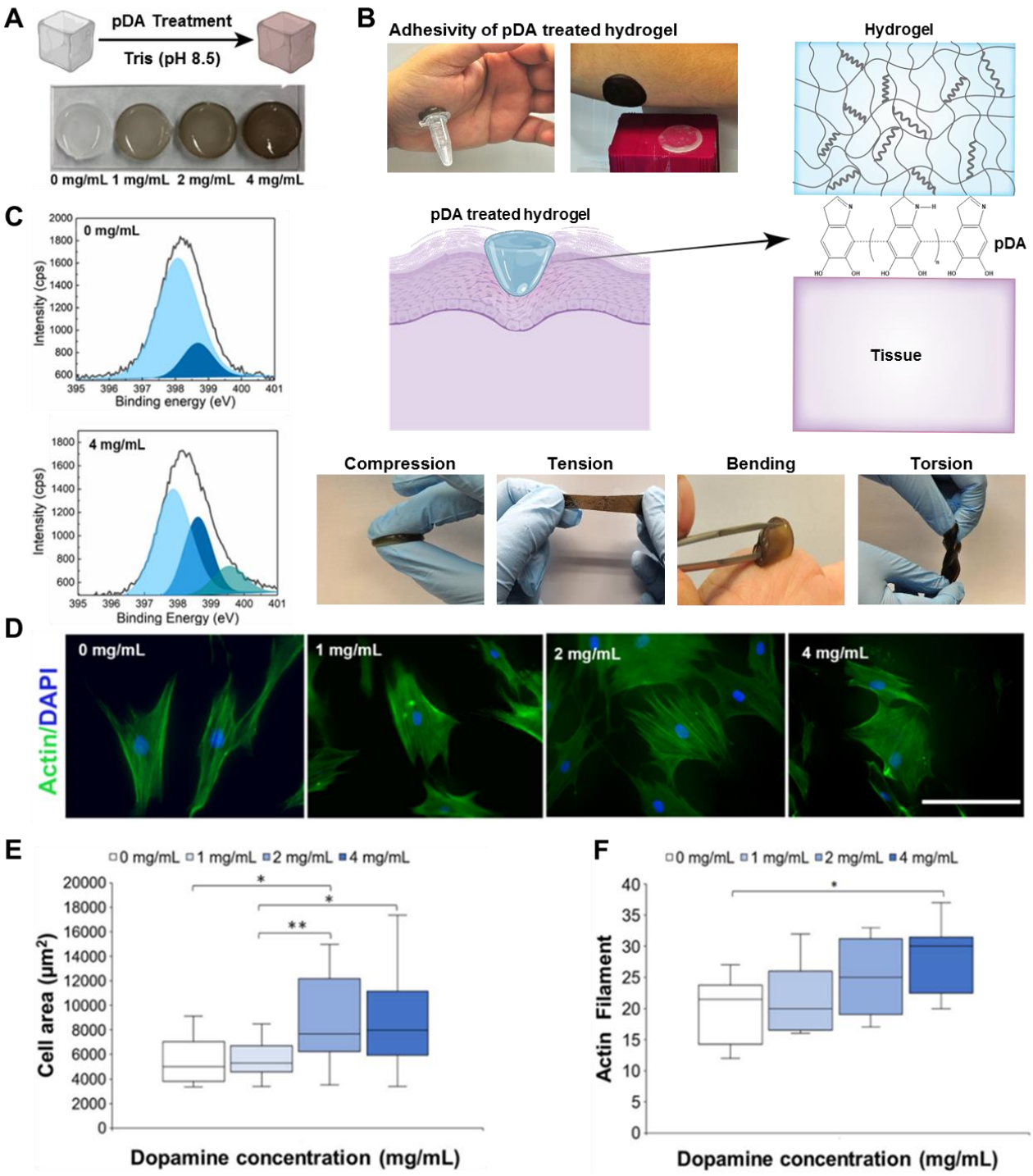

Fig. 3. Effect of pDA-treated Gel-Alg hydrogels on stem cell area and morphology. **A)** The schematic is representing the process of polydopamine formation on the hydrogel surface. Four different concentrations of dopamine were tested. **B)** Images indicate the adhesivity of the polydopamine treated hydrogel. The hydrogel can firmly adhere to the author's palm on one end and a 1.5 ml centrifuge vial (1.03 gm) on the other. However, the untreated hydrogel does not adhere to the skin. The illustration demonstrates wound healing as a possible application of the formulated hydrogel. The polydopamine treatment allows the hydrogel to adhere to tissues. The images in the bottom panel exhibit the behavior of the polydopamine treated hydrogel under compressive, tensile, bending, and torsional stress. **C)** N1s spectra obtained by XPS analysis of the hydrogel surface with and without the polydopamine treatment. **D)** Actin-DAPI staining of hASCs seeded on the surface of hydrogel treated with different dopamine concentrations. Actin was stained with phalloidin-Alexa Fluor 488 (green) and the nuclei with DAPI (blue). Scale bar = 400 µm **E)** Cell area quantification using imageJ of hASCs seeded on the Gel-Alg hydrogels presenting a different concentration of dopamine. Results are reported as mean ± standard deviation (n=10). **F)** The number of actin filament of hASCs cultured on hydrogels presenting a different concentration of dopamine. Results are reported as mean ± standard deviation (n=10). * = $p<0.05$, ** = $p<0.01$.

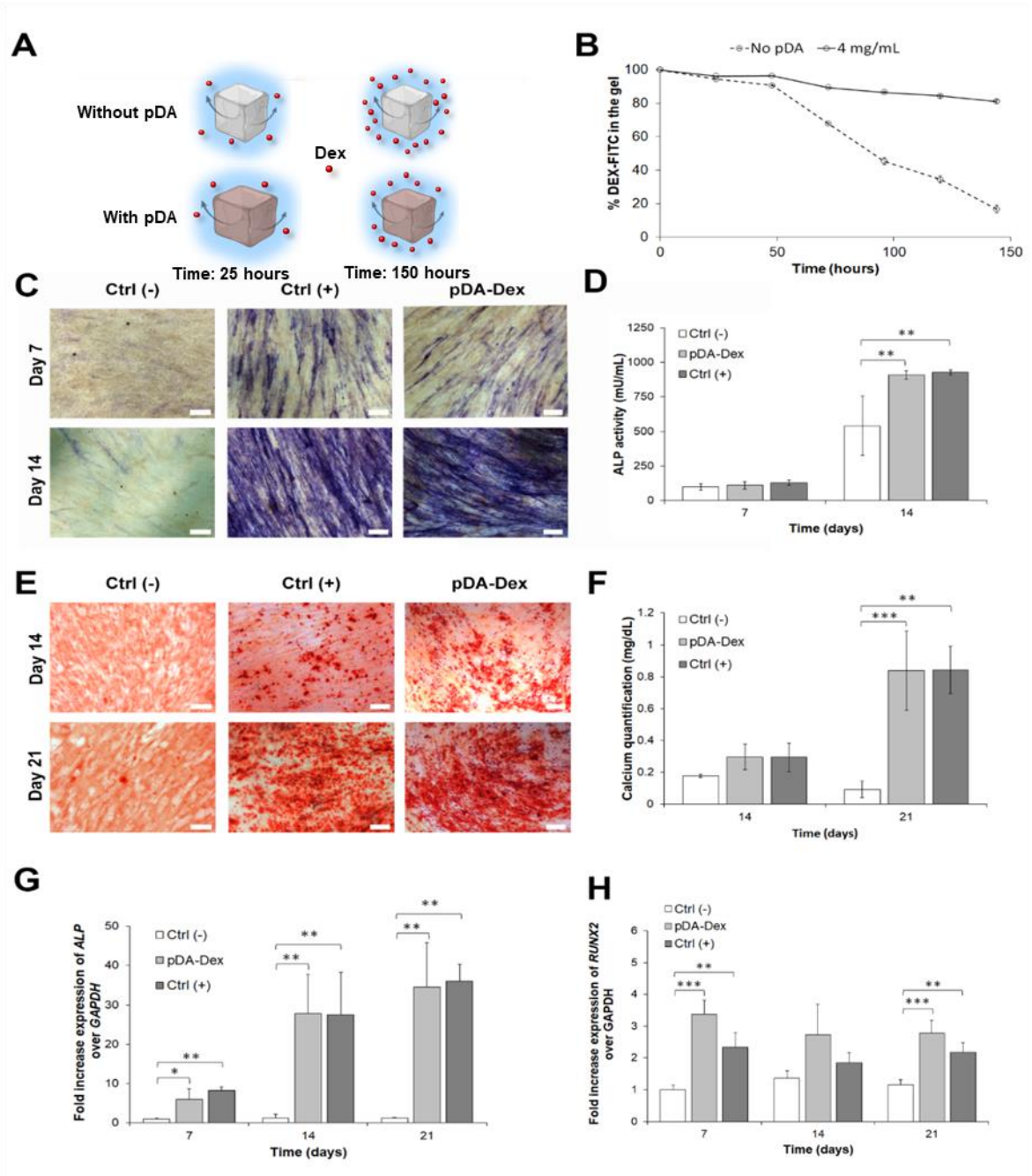

Fig. 4. Modulating stem cell differentiation by sustained release of Dex from pDA-treated Gel-Alg hydrogels. **A)** Schematic indicating the sustained release of Dex in the presence of a pDA-treated hydrogel. Without the pDA treatment, less Dex remains within the hydrogel, whereas, pDA treatment allows the hydrogel to retain more drug. Therefore, a sustained release of Dex occurs with the pDA-treated hydrogel. **B)** Percentage of dexamethasone fluorescein (DEX-FITC) retained by the hydrogel with and without the pDA treatment obtained using 4 mg/mL of a dopamine solution. **C)** Alkaline phosphatase staining of hASCs cultured on different groups at day 7 and 14. Ctrl (-) was the group cultured on hydrogel without any treatment in normal media. Ctrl (+) indicates hASCs cultured on hydrogel without any treatment in osteoinductive media. pDA-Dex represents hydrogels treated both with pDA and dexamethasone. hASCs cultured on this gel were maintained in osteoconductive media. Scale bar = 100 µm. **D)** Quantification of alkaline phosphatase enzymatic activity at 7 and 14 days. Results are reported as mean ± standard deviation (n=5). **E)** Alizarin staining pictures displaying the presence of intracellular calcium deposits after 14 and 21 days. Scale bar = 200 µm F) Corresponding quantification of calcium content assessed after 14 and 21 days. Results are reported as mean ± standard deviation (n=3). **G)** Gene expression of alkaline phosphatase (ALP) at 7, 14 and 21 days. **H)** Gene expression of RUNX2 at 7, 14 and 21 days (n=4). * = $p<0.05$, ** = $p<0.01$ *** = $p<0.001$.

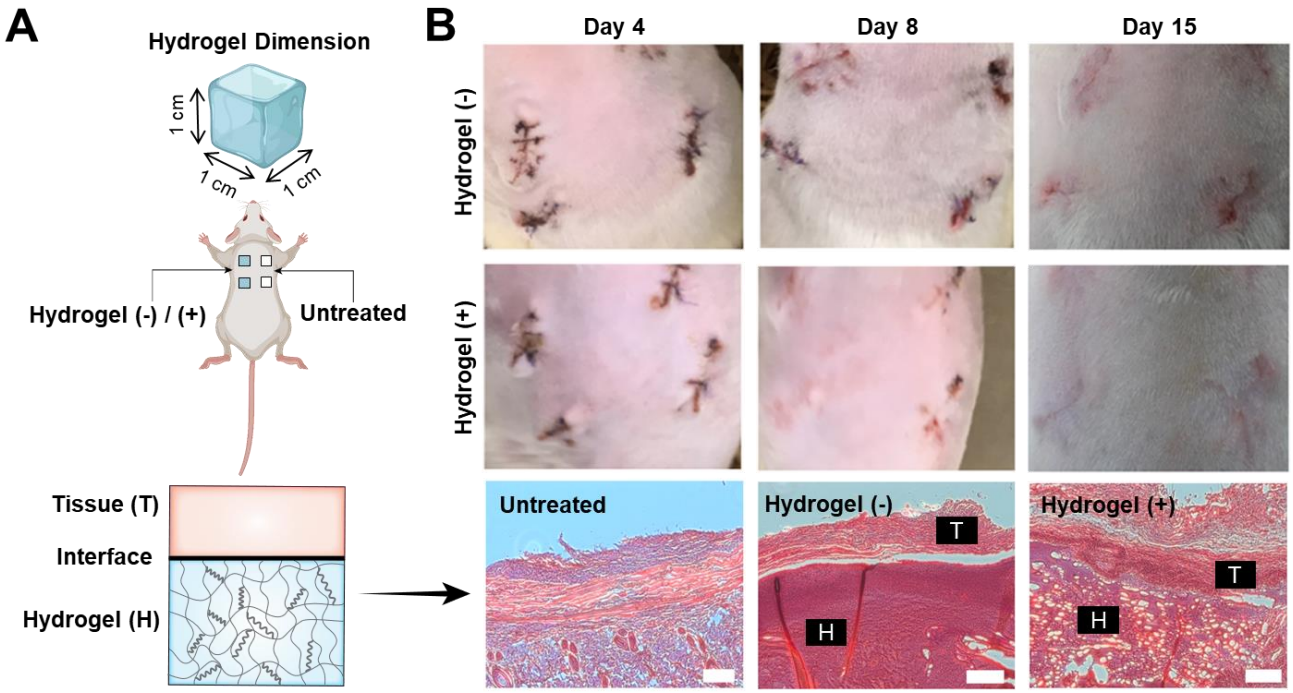

Fig. 5. Assessment of i*n vivo* biocompatibility of pDA-treated Gel-Alg hydrogel. **A)** The schematic represents the study design and different groups investigated in the in vivo analysis. **B)** The wounds on the left were treated with hydrogel. Hydrogel (-) represents Gel-Alg hydrogel without pDA treatment; Hydrogel (+) represents Gel-Alg hydrogel with pDA treatment, supplemented with QK peptide. The wounds on the right were left untreated. On the side, there are the corresponding images of the dorsal side of the rats showing the healing process at the different time points specified. The bottom panel shows H&E staining, which displays the interface between the hydrogel (H) and the tissue (T). The hydrogel without pDA treatment was almost intact after 15 days post-implantation with no sign of cellular infiltration. In contrast, the hydrogel with pDA treatment was largely degraded and porous in appearance. Scale bar = 200 µm.